Circular Waveguide Grating-Via-Grating for Interlayer Coupling

Congshan Wan, *Student Member, IEEE*, Thomas K. Gaylord, *Fellow, IEEE*, and Muhannad S. Bakir, *Senior Member, IEEE*

***Abstract*— A circular waveguide grating-via-grating (GVG) coupler is designed to achieve vertical interlayer optical coupling. Interlayer coupling efficiency is simulated to be 41% (single layer efficiency is 64%) for Si_3N_4 circular waveguide gratings for TE polarization at 1.55-μm wavelength, which is comparable with that of rectangular SOI gratings incorporating adjacent-layer reflectors. The grating ridges of circular gratings are relatively wide (e.g. >465 nm) and adjacent-layer reflectors are not required, both of which simplify fabrication. In-plane circular distributed Bragg reflectors are incorporated to enhance the waveguide-grating interaction. The resonance-enhanced circular gratings are relatively compact compared with the conventional Si_3N_4-based rectangular gratings, e.g., the inner grating is 20 μm in diameter. Furthermore, this GVG coupling structure is less sensitive to misalignment, works well for a wide range of wavelengths (e.g. ±100 nm), and can operate with larger interlayer separations (e.g. ∼5 μm) compared with conventional rectangular gratings.**

***Index Terms*— Circular grating, interlayer coupling, optical interconnect.**

I. Introduction

PHOTONIC interconnects have shown their potential to satisfy the ever-growing need for large bandwidth, low energy, and high data rates. As we move toward heterogeneous multi-die integration within a single-package using 2.5D and 3D IC technologies [1], there is a need for within- and off-package optical connectivity. As such, out-of-plane interlayer optical connectors, such as 45° mirrors, evanescent couplers, and diffraction gratings, are potential candidates to couple optical signals into and out of optical elements on the package and bonded chips. Diffraction gratings are promising because they can achieve relatively large interlayer distances, and their planar geometries make them compatible with integrated circuits and wafer-scale testing. One-dimensional rectangular gratings are commonly used, and several methods have been proposed to increase their diffraction efficiencies. One method is to improve the radiation factor, e.g. engineering grating materials, depth and period [2] as well as reducing back-reflections by apodizing grating fill factors [3]. Another method is to enhance the diffraction directionality, which includes designing asymmetric grating profiles [4], incorporating adjacent-layer reflectors [5], and depositing high-index overlayers [6]. Since the diffraction behavior of 1D/2D rectangular gratings is governed by Floquet theory, specific grating periods have to be defined for particular material systems. For a Si-based waveguide grating at around the 1.55 μm communication wavelength, relatively small grating periods (∼600 nm periods, ∼300 nm grating ridges) are needed. This requires high-resolution fabrication techniques, such as e-beam lithography or deep UV lithography, which may increase the fabrication cost. The methods used to increase the directionality also add complexity to the fabrication process. Furthermore, rectangular grating couplers are sensitive to misalignment [7], which greatly impacts the cost and complexity of the assembly, integration, and packaging processes as well as the overall photonic interconnect performance.

To overcome these challenges, a pair of circular grating couplers together with a high-index via [8] (GVG coupler) is proposed to achieve interlayer optical coupling. The field propagation and diffraction mechanism differ from those of rectangular periodic gratings, and thus relatively wide grating ridges can be used and there is no need to incorporate adjacent-layer reflectors. At 1.55 μm wavelength, the coupling efficiency obtained from the circular grating-via-grating (GVG) couplers (41% interlayer coupling efficiency, 64% single layer efficiency for air-Si_3N_4-SiO_2 waveguides) are comparable to those obtained from the optimized SOI rectangular gratings with adjacent-layer reflectors (e.g. 69% single layer efficiency with reflectors, 50% efficiency without reflectors [9]). Generally, it is challenging for a Si_3N_4-based rectangular grating to achieve such diffraction efficiency at 1.55 μm due to its relatively small refractive index. With the circular grating design, Si_3N_4 can be a competitive candidate for grating fabrication. This is because Si_3N_4 has many advantageous properties such as high optical transparency in the range of visible and near-infrared (NIR), negligible nonlinear losses, high-quality CMOS-compatible fabrication processes, and high material stability. Circular gratings have been widely used in DFB and DBR lasers [10], resonators [11], modulators [12] and fluorescence emission [13]. However, the use of circular gratings in optical interconnect applications has not been treated to the best of our knowledge. In the next section, we will explore this aspect in detail.

II. Circular GVG Coupler Model

Figure 1 shows the structure in which relatively high-index waveguides and a via are configured to couple optical signals between layers separated by an air gap. This structure can be implemented between two separate overlaid chips or embedded within an on-chip interconnect stack. In the second case, the air gap can be replaced by SiO_2, which will cause only small changes to the overall design presented here.

Manuscript received June 6, 2017; revised August 11, 2017; accepted September 11, 2017. Date of publication September 13, 2017; date of current version October 6, 2017. *(Corresponding author: Congshan Wan.)*

The authors are with the School of Electrical and Computer Engineering, Georgia Institute of Technology, Atlanta, GA 30332 USA (e-mail: cwan3@gatech.edu; tgaylord@ece.gatech.edu; mbakir@ece.gatech.edu).

Color versions of one or more of the figures in this letter are available online at http://ieeexplore.ieee.org.

Digital Object Identifier 10.1109/LPT.2017.2752082

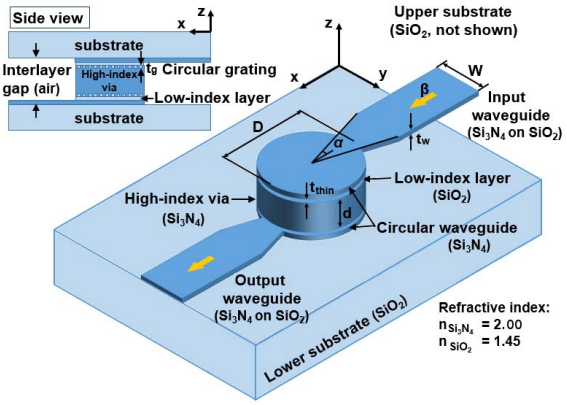

Fig. 1. Schematic representation of the circular grating-via-grating (GVG) coupling configuration. The GVG structure functions to interconnect two layers separated by an air gap.

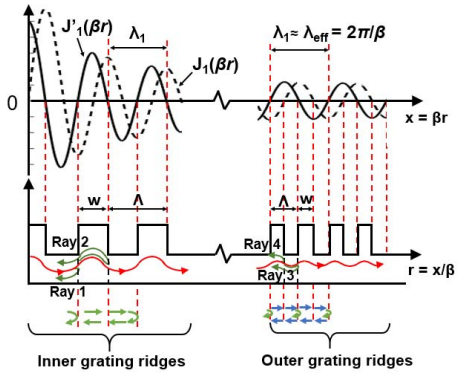

Fig. 2. Circular grating ridge definition and in-plane ray reflection scheme in a circular grating. The green arrows below the grating indicate a phase change of π, and the blue arrows indicate a phase change of $\pi/2$.

Either a TE_z ($E_z = 0$) or TM_z ($H_z = 0$) guided mode is assumed to be introduced into the slab dielectric waveguide. The longitudinal component H_z or E_z, denoted as ψ, satisfies the wave equation. For a circular waveguide, the solution to the wave equation is expressed in cylindrical coordinates as [14]

$$\psi(r,\theta,z) = \sum_{\nu=-\infty}^{\infty} C_\nu J_\nu(\beta r)cos(\gamma z)exp(j\nu\theta), \qquad (1)$$

where ν is the cylindrical mode order, J_ν is the ν-th order Bessel function representing a radial standing wave, β is the radial propagation constant, and γ is the longitudinal propagation constant (z direction) calculated as

$$\gamma = \sqrt{k_0^2 n_w^2 - \beta^2}, \qquad (2)$$

where k_0 is the free-space wave vector ($k_0 = 2\pi/\lambda$, and λ is the free-space wavelength), and n_w is the refractive index of the waveguide layer. The remaining tangential fields (E_r, E_θ, H_r, and H_θ) can be expressed in terms of H_z or E_z through the Maxwell curl equations in cylindrical coordinates. Of particular importance is the E_θ field for TE polarization ($\psi = H_z$), whose direction is tangent to the cylindrical wavefront in the circular waveguide. The E_θ field is expressed as

$$E_\theta = \frac{j\omega\mu_0}{\beta^2} \sum_{\nu=-\infty}^{\infty} C_\nu \frac{d[J_\nu(\beta r)]}{dr} cos(\gamma z)exp(j\nu\theta). \qquad (3)$$

The guided-mode wavelength λ_ν of the ν-th order mode is defined as the difference between two consecutive zeros of the function $d[J_\nu(\beta r)]/dr$, denoted $J'_\nu(\beta r)$, which describes the radial variation of the E_θ field [15] (Fig. 2). As a result, λ_ν is larger at the center and approaches $\lambda_{eff} = 2\pi/\beta_0$ at greater radial distances r, where λ_{eff} and β_0 are the effective wavelength and the transverse propagation constant of a guided mode with a planar wavefront, respectively.

When the circular grating is present, the guided mode in the circular waveguide will be perturbed but β will not be affected, which differs from the case of a rectangular grating whose horizontal propagation constants β_l are modified by the grating through the Floquet condition $\beta_l = \beta_0 - lK$, where l indicates the diffraction order and K is the grating vector magnitude. This is because the radial fields in the circular region, represented by $J_\nu(\beta r)$, are not periodic. Since β is approximately equal to β_0 (e.g. $\beta \approx \beta_0 = 6.7609\ \mu m^{-1}$ given a 340 nm-thick air-Si_3N_4-SiO_2 single-mode waveguide at 1.55 μm wavelength), β is much larger than the wavevector in the cladding (e.g. $k_c = k_0 n_c = 5.8778\ \mu m^{-1}$ for SiO_2 cladding), and thus the longitudinal field $Z(z)$ in the cladding is evanescent, preventing circular gratings from emitting propagating waves and behaving as efficient interlayer couplers. Therefore, a high-index via needs to be incorporated between the two circular gratings to provide an optical path for vertical coupling (Fig. 1). The evanescent behavior in the cladding makes it unnecessary to incorporate reflectors because all the propagating light will only be present in the high-index via.

The circular grating can be divided into two regions. The inner region is designed for field perturbation, and the outer region serves as an in-plane circular distributed Bragg reflector. The arrangement of grating ridges is based on the ray optics concept depicted in Fig. 2, and the phase changes are indicated by the green (phase change of π) and blue (phase change of $\pi/2$) arrows below the grating. Note that the reflected light will experience a phase change of π when it reflects from a medium of higher index and no phase change when it reflects from a medium of lower index. In the inner grating, the radially propagating waves (red rays) constructively interfere if the inner grating periods Λ_i satisfy

$$\Lambda_i = p\lambda_\nu, \qquad (4)$$

and the reflected rays 1 and 2 will be cancelled if the inner grating ridge widths w_i are

$$w_i = \frac{q}{2}\lambda_\nu, \qquad (5)$$

where p and q are arbitrary integers. For convenience, q is set equal to p and thus $w_i = \Lambda_i/2$. The outer grating is designed in such a way that the reflected waves (ray 3 and 4) are enhanced, so the outer grating periods Λ_o are defined as

$$\Lambda_o = \frac{s}{2}\lambda_\nu, \qquad (6)$$

and the outer grating ridge widths w_o need to satisfy

$$w_o = \frac{2t-1}{4}\lambda_\nu, \qquad (7)$$

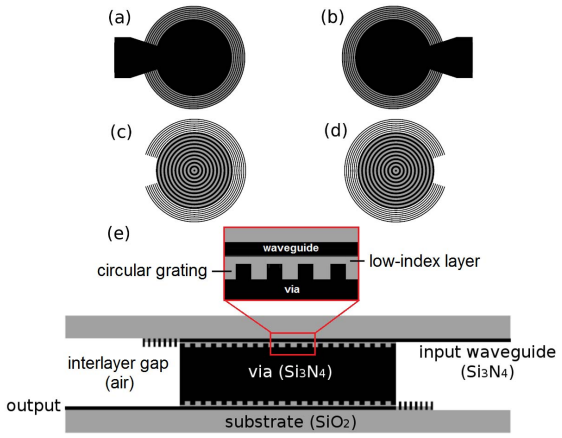

Fig. 3. Cross-sectional views of the coupling structure. Horizontal sections (a)-(d) are bottom waveguide, top waveguide, bottom grating, and top grating, repectively. Vertical section (e) depicts all the layers of the interlayer coupling structure.

where s and t are arbitrary integers. According to the analysis above, the grating period Λ and the grating ridge width w need to be defined locally since λ_ν depends on the radial location. As p, q, s and t can be arbitrary integers, the grating ridges can be relatively wide provided the interference conditions are satisfied.

The cylindrical mode order $\nu = 1$ is chosen to define λ_ν because of its 180° rotational symmetry. According to Eq. (3), the field component $exp(-j\nu\theta)$ with $\nu = 1$ has one nodal line. This field pattern will promote the field coupling from the input waveguide to the output waveguide with minimal loss along the nodal line. By defining the grating ridges based on λ_1, the other mode orders will be suppressed since only the $\nu = 1$ order satisfies the interference conditions. A thin layer of a low-index material is sandwiched between the waveguide and the grating to enhance the in-plane resonance. The field in the input waveguide can be evanescent-coupled to the via and transported to the output grating. The presence of the thin layer impedes the direct propagation from the waveguide to high-index grating ridges and forms another resonant cavity along the z direction. This effectively allows more time for the light to interact with the grating and further suppresses modes other than $\nu = 1$ order. Since the light is initially launched from a rectangular slab waveguide, a waveguide taper is used to convert gradually the plane wavefront in the rectangular waveguide to the cylindrical wavefront in the circular waveguide. The structure is less prone to misalignment because it doesn't follow the "sensitive" Floquet condition.

III. Results and Discussion

Figure 3 shows the cross-sectional views of the coupling structure. Table I summarizes the values of parameters indicated in Fig. 1. A full-wave simulation was performed using 3D FDTD. The waveguides and via are made of Si_3N_4. The low-index layer, made of SiO_2, is sandwiched between the waveguide and the grating layer. The center grating ridges are defined based on Eq. (4) and (5) by using $p = 1$, and the minimum ridge width is 465 nm (period 930 nm),

TABLE I
Parameters for the Circular GVG Coupler

Zeros [a]	r [b](μm)	δr [c](μm)	Parameter [d]	Value
1.8412	0.2723	–	β_0 (μm^{-1})	6.76
5.3314	0.7886	0.5162	t_w (μm)	0.34
8.5363	1.2626	0.4740	t_g (μm)	0.34
11.7060	1.7314	0.4688	t_{thin} (μm)	0.1
14.8636	2.1985	0.4670	W (μm)	10
18.0155	2.6647	0.4662	d (μm)	4.7
21.1644	3.1304	0.4658	λ (μm)	1.55
24.3113	3.5959	0.4655	k_0 (μm^{-1})	4.05
27.4571	4.0612	0.4653	$n_{Si_3N_4}$ [e]	2
30.6019	4.5263	0.4651	n_{SiO_2} [e]	1.45
33.7462	4.9914	0.4650	$k_0 n_{Si_3N_4}$ (μm^{-1})	8.11
36.8900	5.4564	0.4650	$\gamma_{Si_3N_4}$ (μm^{-1})	4.47
40.0334	5.9213	0.4649	ϕ [f](°)	33.5
43.1766	6.3862	0.4649	D_{inner} [g](μm)	19.28
46.3196	6.8511	0.4649	D_{outer} [g](μm)	25.79
49.4624	7.3159	0.4648	δr_{outer} [h](μm)	0.232
52.6050	7.7808	0.4648	N_{inner} [i]	10
55.7476	8.2456	0.4648	N_{outer} [i]	7
58.8900	8.7104	0.4648	p, q	1
62.0323	9.1752	0.4648	t, s	1
65.1746	9.6399	0.4648	α (°)	20

[a] Zeros of $J_1'(x) = d[J_1(x)]/dx$, where $x = (\beta/p)r$;
[b] Locations of grating falling/rising edges as shown in Fig. 2;
[c] Spacing between alternating ridge and groove;
[d] Parameters that specify the GVG structure are shown in Fig. 1;
[e] n represents refractive index;
[f] Diffraction angle in the via $\phi = tan^{-1}(\gamma/\beta)$;
[g] Inner or outer grating diameter;
[h] Outer grating ridge spacing;
[i] Number of inner or outer grating ridges

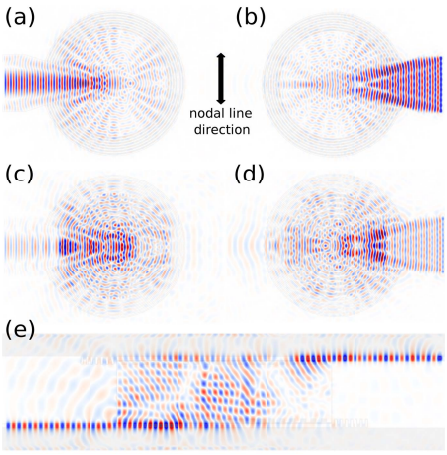

Fig. 4. Cross-sectional views of the H_z field distribution. Horizontal sections (a)-(d) are bottom waveguide, top waveguide, bottom grating, and top grating, repectively. Vertical section (e) depicts the interlayer coupling.

which can be fabricated by photo-lithography. For the outer grating, we set the values of t and s to 1 for demonstration purposes. The inner and outer grating can be treated as a second-order out-coupler and a first-order Bragg reflector, respectively. Larger integer values of p, t and s result in wider grating ridges. Parameter optimization was done on

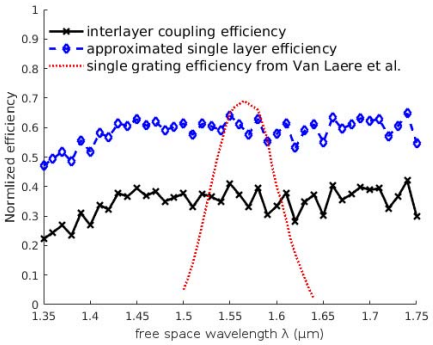

Fig. 5. Wavelength sweep for the designed coupling structure and the rectangular grating reported in [9].

via height d, low-index layer thickness t_{thin}, and taper half-angle α.

The cross-sectional H_z field patterns are shown in Fig. 4. A TE-polarized optical signal is launched from the top waveguide and 41% of that power is coupled into the bottom waveguide. Most of the power loss is due to the field that is adjacent to the bottom waveguide taper which leaks out of the resonant cavity, as shown in Fig. 4(a) and (c). There is also a noticeable amount of back-reflection in the top waveguide, which can be observed from the interference pattern in the top waveguide in Fig. 4(b). A relatively strong field intensity occurs at the junction where the optical signal in the top waveguide reaches the high-index via region, and the propagation angle ϕ in the via is about 33.5° approximated by $\phi = tan^{-1}(\gamma/\beta)$. The coupling distance is relatively large (4.7 μm), which is designed based on the grating dimension and propagation angle in the via. By varying the grating dimension, various coupling distances can be realized. In the current design, the height and the radius of the high-index via are 4.7 μm and 19.28 μm, respectively.

The spectral response of the designed structure is shown in Fig. 5. The coupling efficiency is relatively constant for a wide wavelength range from 1.45 μm to 1.65 μm ($\pm$100 nm). The oscillations in the single-layer and interlayer curves are possibly due to constructive and destructive interference effects. The efficiency eventually decreases at wavelengths much different from the design wavelength (1.55 μm). The wavelength bandwidth for the designed structure is much wider than that of conventional SOI gratings, e.g. 40 nm bandwidth at 1 dB [9], which is also shown in Fig. 5.

IV. Conclusion

A vertical interlayer coupling structure (GVG) is designed by using circular gratings and a high-index via. The coupling structure is compact (~20 μm inner grating diameter), efficient (41% interlayer coupling efficiency, or equivalently, 64% single layer efficiency), and viable over a wide wavelength range. The grating ridges are relatively wide (>465 nm) and no adjacent-layer reflectors are used, which greatly reduce fabrication complexity and cost. Thus the GVG structure represents a promising candidate for an interlayer optical interconnect.

References

[1] A. V. Krishnamoorthy *et al.*, "From chip to cloud: Optical interconnects in engineered systems for the enterprise," in *Proc. 5th IEEE Photon. Soc. Opt. Interconnects Conf.*, May 2016, pp. 34–35.

[2] C. Wan, T. K. Gaylord, and M. S. Bakir, "Grating design for interlayer optical interconnection of in-plane waveguides," *Appl. Opt.*, vol. 55, no. 10, pp. 2601–2610, Apr. 2016.

[3] X. Chen, C. Li, C. K. Y. Fung, S. M. G. Lo, and H. K. Tsang, "Apodized waveguide grating couplers for efficient coupling to optical fibers," *IEEE Photon. Technol. Lett.*, vol. 22, no. 15, pp. 1156–1158, Aug. 1, 2010.

[4] C. Wan, T. K. Gaylord, and M. S. Bakir, "RCWA-EIS method for interlayer grating coupling," *Appl. Opt.*, vol. 55, no. 22, pp. 5900–5908, Aug. 2016.

[5] G. Roelkens, D. Vermeulen, S. Selvaraja, R. Halir, W. Bogaerts, and D. Van Thourhout, "Grating-based optical fiber interfaces for silicon-on-insulator photonic integrated circuits," *IEEE J. Sel. Topics Quantum Electron.*, vol. 17, no. 3, pp. 571–580, May/Jun. 2011.

[6] G. Roelkens, D. Van Thourhout, and R. Baets, "High efficiency silicon-on-insulator grating coupler based on a poly-silicon overlay," *Opt. Exp.*, vol. 14, no. 24, pp. 11622–11630, Nov. 2006.

[7] C. Wan, T. K. Gaylord, and M. S. Bakir, "Rigorous coupled-wave analysis equivalent-index-slab method for analyzing 3D angular misalignment in interlayer grating couplers," *Appl. Opt.*, vol. 55, no. 35, pp. 10006–10015, Dec. 2016.

[8] M. S. Bakir, T. K. Gaylord, O. O. Ogunsola, E. N. Glytsis, and J. D. Meindl, "Optical transmission of polymer pillars for chip I/O optical interconnections," *IEEE Photon. Technol. Lett.*, vol. 16, no. 1, pp. 117–119, Jan. 2004.

[9] F. V. Laere *et al.*, "Compact and highly efficient grating couplers between optical fiber and nanophotonic waveguides," *J. Lightw. Technol.*, vol. 25, no. 1, pp. 151–156, Jan. 2007.

[10] C. Wu *et al.*, "Threshold gain and threshold current analysis of circular grating DFB and DBR lasers," *IEEE J. Quantum Electron.*, vol. 29, no. 10, pp. 2596–2606, Oct. 1993.

[11] J. Scheuer and A. Yariv, "Coupled-waves approach to the design and analysis of Bragg and photonic crystal annular resonators," *IEEE J. Quantum Electron.*, vol. 39, no. 12, pp. 1555–1562, Dec. 2003.

[12] N. Moll *et al.*, "Circular grating resonators as micro-cavities for optical modulators," in *Proc. 4th IEEE Int. Conf. Group IV Photon.*, Sep. 2007, pp. 1–3.

[13] M. Davanço, M. T. Rakher, D. Schuh, A. Badolato, and K. Srinivasan, "A circular dielectric grating for vertical extraction of single quantum dot emission," *Appl. Phys. Lett.*, vol. 99, no. 4, p. 041102, Jul. 2011.

[14] C. Wu, T. Makino, J. Glinski, R. Maciejko, and S. I. Najafi, "Self-consistent coupled-wave theory for circular gratings on planar dielectric waveguides," *J. Lightw. Technol.*, vol. 9, no. 10, pp. 1264–1277, Oct. 1991.

[15] R. M. Schimpe, "Cylindrical diffraction grating couplers and distributed feedback resonators for guided wave devices," U.S. Patent 4 743 083, May 10, 1988.